Hindawi
Advances in Civil Engineering
Volume 2019, Article ID 8132817, 13 pages
https://doi.org/10.1155/2019/8132817

Research Article

Research on Failure Mechanism and Strengthening of Broken Roadway Affected by Upper Coal Pillar

Fulian He,[1,2] Zheng Zheng ,[1] Hengzhong Zhu,[1] and Bo Yang[1]

[1]*College of Resources & Safety Engineering, China University of Mining & Technology (Beijing), Beijing 100083, China*
[2]*Beijing Key Laboratory for Precise Mining of Intergrown Energy and Resources, China University of Mining & Technology (Beijing), Beijing 100083, China*

Correspondence should be addressed to Zheng Zheng; 1422308269@qq.com

Received 4 September 2018; Revised 3 January 2019; Accepted 24 January 2019; Published 1 April 2019

Academic Editor: Hugo Rodrigues

The principal stress difference is introduced as a new evaluation index in order to better understand the failure mechanism of roadways affected by upper coal pillars and characterize failure of rock mass. Compared with traditional methods, it facilitates quantitative analysis. Moreover, we combine the semiplane theory and we obtain the stress distribution on the coal pillar's bedrock and the strengthening control area from the "change point" position along a 21 m horizontal line. The influence of multiple stresses induced from mining on a roadway is analyzed. It is found that rock failure is most likely while mining the 051606 working face, followed by mining the 051604 working face, and the stress influence on the upper pillar has the lowest failure probability. In addition, based on the asymmetry of the surrounding rock stress distribution, this study proposes strengthening control technology of surrounding rock on the basis of a highly stressed bolting support and anchor cable, adding to the steel ladder beam, steel mesh, and shed support's protective function to the roadway's roof and ribs. Finally, through field observations, it is concluded that the roadway deformation is within the controllable range.

1. Introduction

In recent years, with the increasing use of energy, China's annual coal production has accounted for nearly half of the world's production [1–3]. Moreover, it brings a solid energy foundation for national economic construction [4–6]. In China, with the increase of mining intensity, more and more close coal seams are being mined [7]. In the close-up coal seam, the upper coal seam will leave the coal pillar after mining, and the overlying stratum load will produce stress concentration on these pillars, which will directly affect the integrity and strength of the lower coal roof [8]. Especially, when the roadway in lower coal crosses the pillar of the upper coal seam in space, it greatly increases the difficulty of supporting in the lower coal seam roadway. If the supplement support parameters cannot be reasonably selected, it is likely to lead to large-scale roof caving in this roadway.

Experts and scholars have done a lot of research on the characteristics of strata behavior in the close distance seam mining. Lu et al. [9, 10] explained the quantitative relationship between Z and X. The vertical distance between the roadway and the upper coal seam is Z. And the horizontal distance between the roadway and the edge of the upper coal pillar is X, which provided the main basis for correctly selecting the X value and the relative position relationship between the roadway and the upper coal seam mining space. Guan and Li [11] calculated the distribution of stress, displacement, and failure area of surrounding rock after coal mining, obtaining the limit load of floor rock mass and the empirical formula for calculating the maximum failure depth of coal seam floor. Zhang and Zhang [12] in multi coal seam joint mining research, determined the distance of outward alternate entries as 12–14 m by using FLAC3D numerical simulation software to simulate the change of stress and displacement in roof floor and two sides of roadway. Wilson [13] analyzed the stability factors of soft rock roadway and comprehensively discussed the failure mechanism of soft rock under the influence of coal pillar width and working face mining. Xu and Zhang [14] considered that the main cause of roadway failure in the lower coal seam was the principal stress difference. Li et al. [15] set

the gob as strain hardening model and the coal pillar as strain-softening model according to the actual mechanical characteristics of coal and rock mass. The accuracy of the numerical model is greatly improved. Sui et al. [16] proposed a new index "Dividing Line D" to define the overburden failure state and using it to discuss the interactions of overburden damage zones in close-up coalbed mining. Zhu [17] established the mechanics model of breaking block structure of key seam and analyzed the influence of breaking line position in upper coal seam roof on the structural stability in lower coal seam. An underground engineering is generally a complex dynamical system. The important work during mining is to control the deformation of coal mine roadway and coal-face. In essence, the mine deformations are the final result of the interaction of some disaster factors. In 2000, Qiao [18, 19] dealt with the converse theorem of the Leau-Fatou petal theorem on complex dynamical systems and revealed an impressive rule which said that the geometrical properties of the unstable set could impact the structural stability of dynamical systems directly.

Scholars have been exploring failure of surrounding rock and strata after close-up coal seam mining for a long time. Generally, the reasonable location of the working face and roadway in lower coal is the primary focus of this research. However, under the influence of boundary pillars in upper coal seam areas, there is relatively little research on the roadway crossing through this boundary pillar section in the lower coal seam. Under these conditions, the strengthening control area cannot be determined directly. In addition, using vertical stress to characterize failure of surrounding rock in traditional research is inappropriate. Therefore, according to the relative position of the Mohr circle and envelope curve, it is more scientific to use "principal stress difference" to quantify the integrity of the surrounding rock.

2. Engineering Background

The 051606 working face, 265 m average depth, is located in the 16 coal seam of the fifth mining area in the Ling Xin Coal Mine, Ningxia Province, China. The eastern part is 560 m apart from the fault, the southern side is about 204 m away from the exploration line, the western side and the 051604 working face have 20 m protective coal pillars, and the distance from the northern side to rail rise of the fifth mining area is about 46 m. #15 coal seam exploited is about 21 m above the 051606 working face. Therefore, in the process of driving 051606 ventilation roadway, it crosses through successively the 051504 goaf, the 35 m boundary pillar, and W1415 goaf in space. The 20 m protective coal pillar is left between 051504 goaf and 051506 goaf, as well as 051604 goaf and 051606 working face. Its space position is shown in Figure 1. #16 coal seam is medium thick coal seam, its average thickness in the working face area is 5.02 m, and the roof is a harder silt and fine sandstone. The section of the roadway under the influence of the upper boundary pillar has a stronger strata behavior. That is "special failure section" in Figure 1. Through field observation, the roadway's roof of the most serious section had obvious step subsidence, the two shoulder angles were damaged seriously, some bolt pallets failed, and part of anchor cable had the phenomenon of breaking. The others' roadway is placed on the underside of the upper coal seam goaf, which is basically in a low stress state. Its surrounding rock is relatively complete and can satisfy pedestrians and transportation functions.

3. Principal Stress Difference

3.1. Stress Transfer Model. In order to analyze the influence of stress on the upper coal pillar and goaf, we use the semiplane theory from elastic mechanics [20] to calculate the stress in the coal and rock mass below. At this time, the boundary pillar forms the border between two adjacent mining areas. As the two sides of the working face are pushed forward, the roof breaks in the form of "O-X" [21]. According to reliable data obtained from numerous field experiments, the goaf experiences the same stress as virgin rocks when it is about 0.12 to 0.3 times of the buried depth from the edge of coal pillar [21]. In other words, the original rock stress begins to appear about 35–90 m into the goaf. The effect of stress is only analyzed 60 m into the goaf in this study. The mechanical model in Figure 2 can be used to describe this situation, where X points vertically and Y points horizontally.

In order to simplify the calculation without sacrificing accuracy [22], rock in the upper seam floor is assumed to be affected by the superposition of L_1, L_3 gobs, and L_2 boundary pillar, where the total pressure from these three loads can be calculated at point M. Under the influence of concentrated stress q_1 by L_1 gob, stress at point M (r, θ) in the bedrock is shown as follows [20]:

$$\sigma_x^1 = \frac{2q_1\cos^3\theta}{r\pi},$$
$$\sigma_y^1 = \frac{2q_1\cos\theta\sin^2\theta}{r\pi}, \quad (1)$$
$$\tau_{xy}^1 = \frac{2q_1\cos^2\theta\sin\theta}{r\pi}.$$

In this formula, σ_x^1, σ_x^1, and τ_{xy}^1 are the vertical, horizontal, and shear stress components at M under the influence of L_1 gob, respectively, and q_1 is the uniform load value in L_1 gob. A small length $d\eta$ is selected at the coordinate η on the x-axis ($0 \le x \le L_1$), and its uniform load is $q(\eta) = \lambda_0\gamma H$. Therefore, the vertical and horizontal distances between M (x, y) and η are x and $(y - \eta)$, respectively. The differential stress $d\eta$ at M is defined as follows:

$$d\sigma_x^1 = -\frac{2\lambda_0\gamma H\ d\eta}{\pi}\frac{x^3}{\left[x^2 + (y-\eta)^2\right]^2},$$
$$d\sigma_y^1 = -\frac{2\lambda_0\gamma H\ d\eta}{\pi}\frac{x(y-\eta)^2}{\left[x^2 + (y-\eta)^2\right]^2}, \quad (2)$$
$$d\tau_{xy}^1 = -\frac{2\lambda_0\gamma H\ d\eta}{\pi}\frac{x^2(y-\eta)}{\left[x^2 + (y-\eta)^2\right]^2},$$

where λ_0 is the L_1 gob stress concentration factor, γH is the initial crustal stress of #15 coal seam, and x and y are the

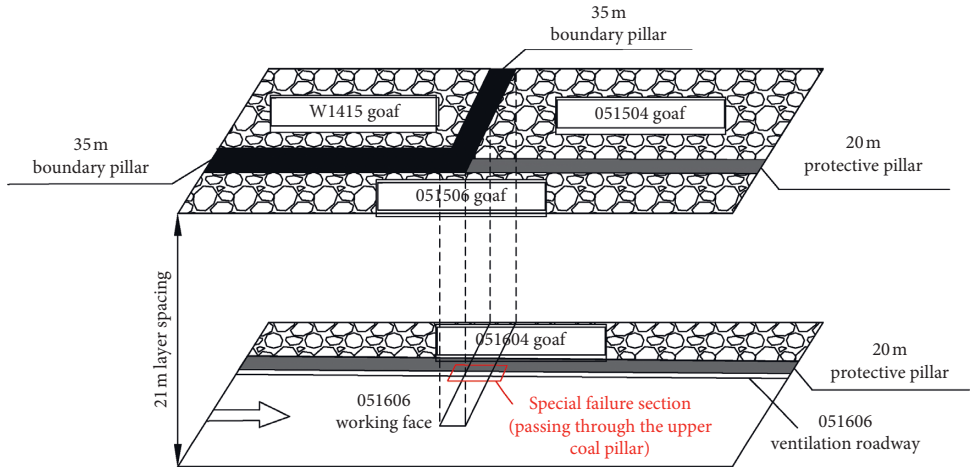

Figure 1: The relationship of space arrangement between the 051606 working face and the upper coal.

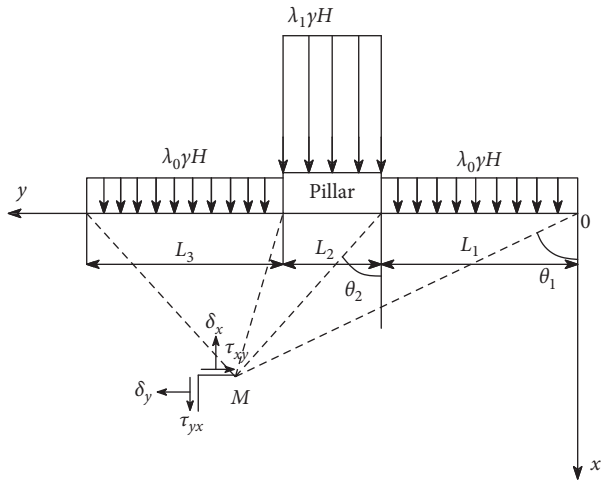

Figure 2: Load transfer model of the boundary coal pillar.

coordinates of M. The stress produced by L_1 gob at M is defined as follows:

$$\sigma_x^1 = -\frac{2\lambda_0\gamma H}{\pi}\int_0^{L_1}\frac{x^3}{\left[x^2+(y-\eta)^2\right]^2}d\eta,$$

$$\sigma_y^1 = -\frac{2\lambda_0\gamma H}{\pi}\int_0^{L_1}\frac{x(y-\eta)^2}{\left[x^2+(y-\eta)^2\right]^2}d\eta, \quad (3)$$

$$\tau_{xy}^1 = -\frac{2\lambda_0\gamma H}{\pi}\int_0^{L_1}\frac{x^2(y-\eta)}{\left[x^2+(y-\eta)^2\right]^2}d\eta,$$

where L_1 is the gob length in the mechanics model. As we can see, the stress from L_1 gob at M can be obtained. Similarly, the stress of the L_2 boundary pillar and L_3 goaf at M can be calculated.

3.2. Principal Stress Difference Analysis. The traditional semiplane theory is usually used to calculate the vertical, horizontal, and shear stresses, but it is obviously difficult to analyze the stress on coal and rock mass using three independent stress components due to the complicated conditions and stress transfer characteristics. Based on Mohr's circle [23], it is proposed that the dilatancy deformation of coal and rock mass be analyzed using the principal stress difference $(\sigma_1-\sigma_3)$. In Figure 3, it is assumed that the stress components of the block element are $(\sigma_x-\tau_{xy})$ and $(\sigma_y-\tau_{xy})$, which satisfy

$$\begin{aligned} p &= \left(\sigma_x+\sigma_y\right)/2,\\ r &= \sqrt{\left[\left(\sigma_x-\sigma_y\right)/2\right]^2+\tau_{xy}^2},\\ \sigma_1 &= p+r,\\ \sigma_3 &= p-r,\\ \left(\sigma_1-\sigma_3\right)_k &= 2r = 2\sqrt{\left[\left(\sigma_x^k-\sigma_y^k\right)/2\right]^2+\left(\tau_{xy}^k\right)^2}, \end{aligned} \quad (4)$$

where p is the average stress, r is the radius of this circle, σ_1 and σ_3 are the maximum and minimum principal stresses, respectively, $\sigma_1-\sigma_3$ is the principal stress difference, and index k refers to segments 1, 2, and 3.

The shear strength of rock mass (τ) does not depend on σ_2 when the cohesion (c) and internal friction angle (φ) are given. Moreover, the principal stress difference $(\sigma_1-\sigma_3)$ determines whether equilibrium is reached. In other words, σ_3 is smaller when σ_1 is constant, thus the probability of failure is larger. When σ_3 is constant, the rock mass is more likely to fail if σ_1 is larger. Therefore, the principal stress difference can be used to directly determine rock mass failure. This is directly incorporated into the stress transfer model, which overcomes the deficiency that the traditional model cannot be used to quantitatively analyze pressure. Moreover, it is more intuitive in judging the stability of a rock mass structure.

According to the special conditions and stress characteristics in this coal seam, the boundary pillar is set to 35 m, and the average buried depth of #15 coal seam is 244 m, thus the crustal stress is about 6 MPa. Considering the stress distribution after coal seam mining, the stress concentration

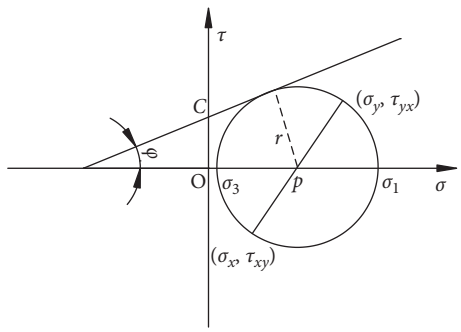

Figure 3: Mohr's circle describing the stress state.

coefficient in the two-sided gobs and boundary pillar is 0.5 and 1.4, respectively [22]. MATLAB was used to solve equation (3) using superposition, yielding the principal stress difference distribution shown in Figure 4. A monitoring line is placed every 3 m along the direction of #15 coal seam floor. The principal stress difference at different depths in the bedrock is shown in Figure 5.

Figures 4 and 5 show the following:

(1) The principal stress difference distribution in the floor of #15 coal seam exhibits a fan-shaped diffusion. The principal stress difference is high at the two ends of the boundary pillar, and stress gradually transfers downward along these two points. The stress gradually decreases and the diffusion range increases as the buried depth increases. Due to pressure relief in the shallow rock mass of the gob floor, the principal stress difference increases gradually from 0 MPa to its maximum value, and the maximum value occurs at a depth of 20 m. The principal stress difference subsequently decreases to a minimum value due to the influence of buried depth.

(2) The depth curve at 0–18 m exhibits two peaks, where the peak positions are at each end of the boundary pillar. As the buried depth increases, the two peaks converge into a single peak, which begins to appear at the position of #16 coal roof (buried depth of 21 m). At this time, the peak principal stress difference value is 5.6 MPa. The peak position appears in the middle of the upper coal pillar. The maximum failure plane will be at the peak position if the 051606 roadway is excavated at this depth. When the depth is greater than 21 m, the peak value decreases and the stability of the coal and rock mass is obviously improved.

(3) There are unique envelope curves at different depths, which directly reflect the principal stress difference distribution at the rock mass boundary in this area. In other words, the numerical value on this envelope curve represents the maximum failure probability at this location. Obviously, when the stress exceeds this range, the rock mass will inevitably experience extremely strong plastic deformation. Due to stress diffusion, the high stress range at the position of #16

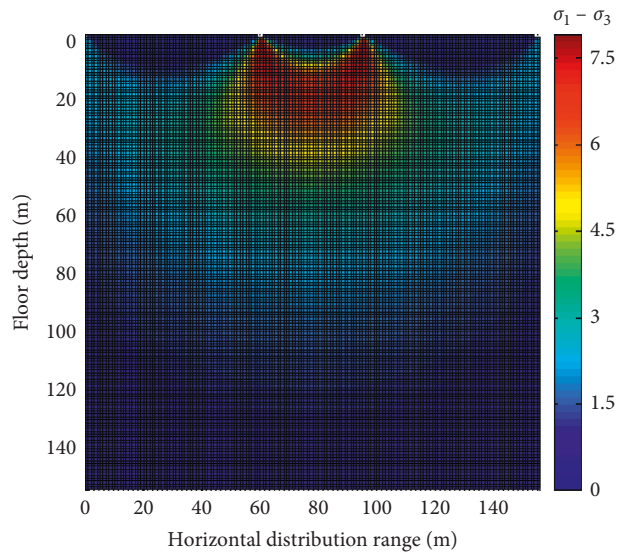

Figure 4: Distribution of principal stress difference in bedrock.

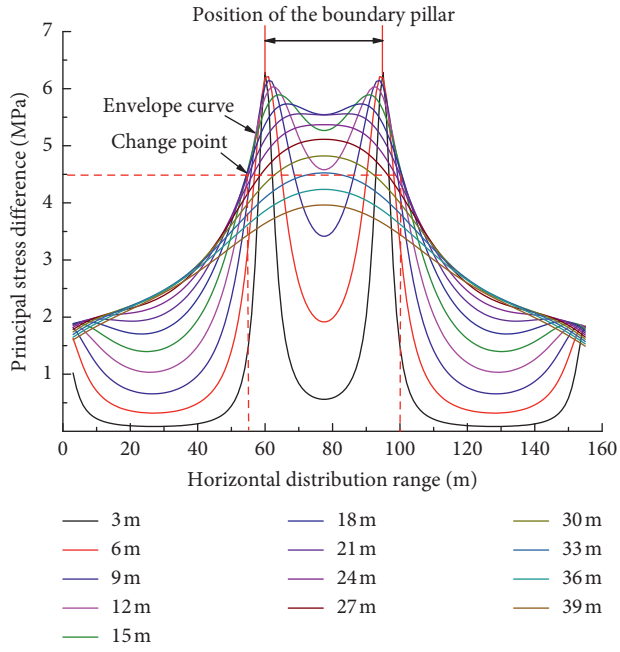

Figure 5: Principal stress difference curves at different depths.

coal roof (buried depth of 21 m) increases evidently. The curve corresponding to a burial depth of 21 m suddenly deviates from the envelope curve and forms a change point. This point is a critical point that indicates when the dilatancy failure degree begins to change from gob-dominant to boundary pillar-dominant. When the upper boundary pillar is dominant, it is also more reasonable to regard the range between the two change points as a strengthening control area. Later, it is called the special failure section in the 051606 ventilation roadway. According to Figure 5, the change point

pressure on #16 coal roof position (buried depth of 21 m) is about 4.5 MPa. Furthermore, from a safety standpoint, the scope of the reinforced support in this roadway under the influence of boundary coal pillar should be increased to 45 m, with the coordinate axis 55–100 m.

4. Numerical Simulation in FLAC3D

4.1. Numerical Model. The 051606 ventilation roadway is primarily affected by the mining area boundary pillar in #15 coal seam, 051604 goaf, and 051606 working face in #16 coal seam. In order to simplify the calculation process and obtain an objective research rule, the influence area of W1415 and 051504 goaf is set to 60 m. The size of the model is $140 \times 156 \times 65\,m^3$, and constrained displacement boundary conditions are defined at the bottom and all around. Overburden stress is applied to the upper part of this numerical model as the stress boundary of the external load. Figure 6 shows the numerical model of the coal seam. The roof collapsed and formed the coal gangue in the goaf, which plays an important role in supporting roof. As the porosity decreases after compaction, and the carrying capacity of gangue is also greatly increased, exhibiting obvious strain-hardening characteristics. Therefore, it is more appropriate to describe the goaf as double-yield model [24]. In addition, the remaining coal and rock masses are all set as Mohr-Column models, and their mechanical parameters are shown in Table 1.

4.2. Failure Mechanism of Surrounding Rock. During the process of close-up coal seam mining, mining of the working face in the upper coal seam influences the stress on the rock surrounding the lower coal seam. The drastic stress field gradually tends to stabilize over time. While tunneling the 051606 ventilation roadway, deformation of the rock surrounding the roadway is more complicated under the support pressure influence by upper boundary pillar and the 051604 adjacent gob. Therefore, we can analyze the deformation in the surrounding rock and roadway failure based on the coal seam mining sequence. The surrounding rock fracture mechanism and stress evolution characteristics under this influence of multiple mining-induced stresses can be obtained, which helps determining the optimal roadway support parameters.

4.2.1. Effect of #15 Coal Seam Mining on #16 Coal Seam. #15 and #16 coal seams are 21 m apart and belong to the close-up coal seam. Before mining the lower coal seam, the stress environment of the surrounding rock was damaged due to mining-induced stress in the upper coal seam, and pressure becomes concentrated in the bedrock of upper boundary pillar [25]. In order to study deformation and failure of the surrounding rock under the influence once #15 coal seam is mined-out, we can use the principal stress difference to characterize the integrity of the coal and rock mass [14]. We monitored σ_1 and σ_3 of the rock mass in #16 coal seam floor, roof, and 7 and 14 m above #16 coal seam roof. A 3D principal stress difference map was built

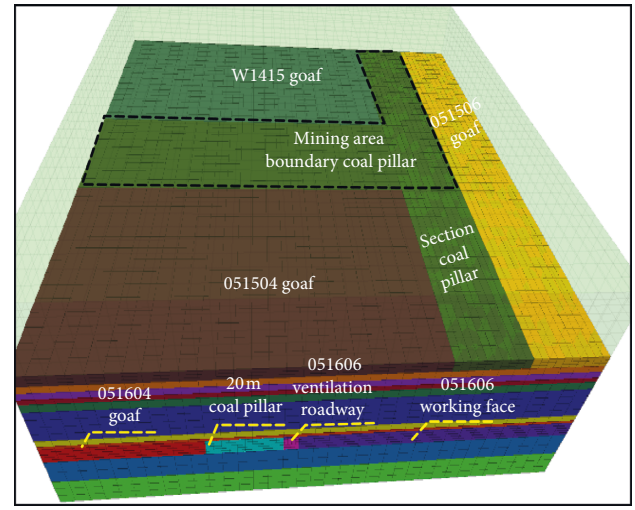

Figure 6: Initial numerical model.

using the postprocessing software-SURFER, as shown in Figure 7.

Figures 7(a)–7(d) show the following:

(1) The principal stress difference peak value in #16 coal seam floor reaches 3.5 MPa (see Figure 7(a)) and that at the roof reaches 4.4 MPa (see Figure 7(b)) due to the residual support pressure of the upper coal seam, and the peak position is basically distributed in the middle of the boundary coal pillar floor. This section's surrounding rock has already undergone a certain degree of dilatancy failure. Later excavation of the 051606 ventilation roadway and working face mining near this section may result in more serious strata behavior like roof leakage and an increased anchor cable failure rate.

(2) Figure 7(c) shows that the high stress area exhibits two peaks. The higher peak position is basically at the edge of the boundary pillar. In addition, the upper boundary pillar is a large pillar with a width of 35 m, and there is an elastic core area with a certain width in the middle of the pillar. Therefore, rock pressure under the floor of the elastic core area is relatively small. However, both sides of the boundary coal pillar, such as the arch foot position of the fracture arch, bear the greatest weight from the overburden strata in the goaf. The rock surrounding both sides of the pillar experiences larger crushing deformation.

(3) The principal stress difference in the strata is greater and is much more strongly influenced by upper coal mining when the distance to the upper coal seam is closer. The principal stress difference curve gradually transforms from one peak to two peaks, which is basically consistent with the transmission state derived from the semiplane theory. However, there is a certain difference in the peak principal stress difference value, which is due to the rock mass characteristics. According to the layered theory [24], compared with a single rock in semiplane theory, the additional stress near the middle axial line undergoes

Table 1: Mechanical parameters of coal and rock mass.

Rock stratum	Density (g/cm^3)	Bulk modulus (GPa)	Shear modulus (GPa)	Cohesion (MPa)	Internal friction angle (°)	Thickness (m)
Silt	2.65	9.1	7.8	7.2	34	3.5
Fine sand	2.7	13.3	10	10.2	37	4.5
Medium sand	2.34	12.3	9.1	5.2	37	11
#15 coal seam	1.3	5	2.08	1.68	28	3
Silt	2.65	9.1	7.8	7.2	34	2
Fine sand	2.7	13.3	10	10.2	37	2
Sandy mudstone	2.63	12.5	10	10	35	1.5
Medium sand	2.34	12.3	9.1	5.2	37	2.5
Coarse sand	3.05	9.9	10.6	10.8	34	10
Silt	2.65	9.1	7.8	7.2	34	2
Mudstone	2.24	3.2	6.69	8.1	36	1
#16 coal seam	1.3	5	2.08	1.68	28	5
Fine sand	2.7	13.3	10	10.2	37	8
Silt	2.65	9.1	7.8	7.2	34	9

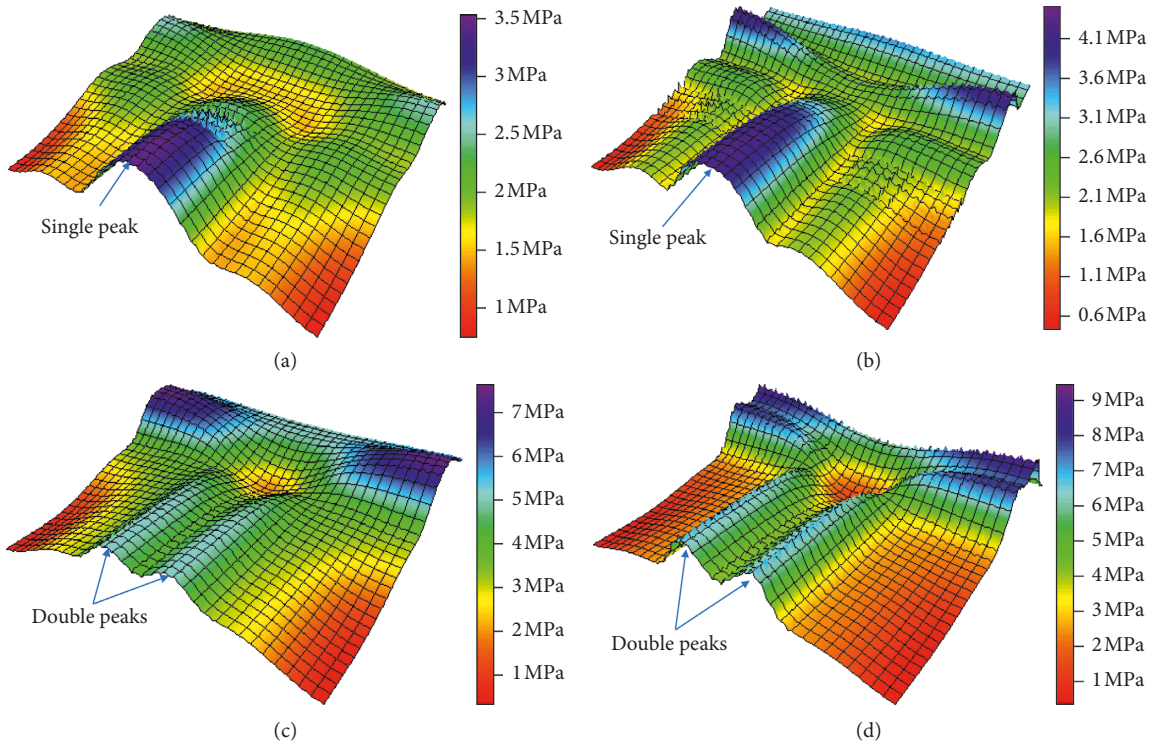

Figure 7: Distribution of principal stress difference under the upper coal floor. (a) #16 coal seam floor. (b) #16 coal seam roof. (c) 7 m above #16 coal seam. (d) 14 m above #16 coal seam.

stress diffusion when the hard layer covers the soft layer in the actual numerical model. In other words, the stress distribution is slightly higher at the two sides than in the middle, as shown in Figure 8. At this time, the floating range is basically controlled within 20~25%, thus the theoretical results are consistent with simulation results.

In summary, because the distance between the two coal seams is 21 m, the stress decreases as stress transfers downward layer-by-layer. Though the rock surrounding the special failure roadway is destroyed under due to upper seam mining to a certain extent, it can still satisfy the basic functions of a roadway if roadway deformation is maintained by reasonable supports. Therefore, reasonable supports and scientific mining methods are particularly important.

4.2.2. Influence of 051604 Goaf on Special Failure Roadway. When the upper coal seam is mined, the dynamic pressure is fully released in the coal and rock mass after a period of time. While mining the lower coal seam, the 051604 working face is mined first, and miners subsequently apply a widely used layout where 20 m coal pillars are used to protect the roadway. At this time, under the superposition of the 051604

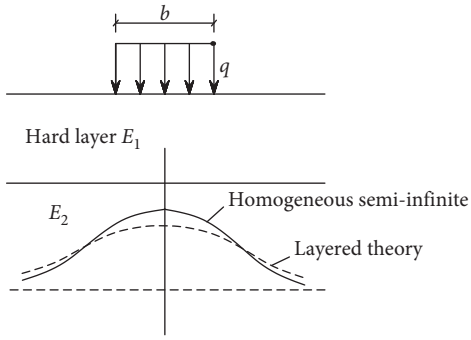

Figure 8: Stress diffusion when $E_1 > E_2$.

adjacent goaf and the upper boundary pillar, the roof and rib of the coal pillar side in the special failure section are seriously damaged. In order to explore the effect of the 051604 adjacent goaf, mining of #15 and #16 coal seams and mining of only #16 coal seam are simulated (Figure 9). Furthermore, according to the analysis of the upper section, the peak position is in the middle section due to the boundary pillar influence. Therefore, deformation of the surrounding rock in this section with the most serious damage (the middle position of the boundary coal pillar) is studied further. This will be named the maximum failure plane later.

An analysis of the maximum failure plane (upper boundary coal pillar, middle line position) shows the following:

(1) Three monitoring lines on the roadway roof show that the principle stress different on the roof of the coal pillar side is the largest, followed by the midline, and the roof of the virgin coal side is the smallest after mining #15 and #16 coal seams (see Figure 9(a)). The load is significantly asymmetric and results in failure of the roof surrounding rock, while the principal stress difference on the virgin coal side decreases gradually. One can see that the shallow coal is fragmented, and the deep coal tends to be stable. The principal stress difference distribution in the coal pillar is bimodal, and the peak value on the goaf side is much higher than that on the roadway side.

(2) The principal stress difference on the rock surrounding the roof and virgin coal exhibits negative index after mining the 051604 working face (see Figure 9(b)). Their maximum principal stress difference is 8 MPa. Figure 9(a) shows that the principal stress difference increases by 2–4 MPa at the same position. Meanwhile, the damage in the coal pillar mass is the most remarkable. The peak value near the roadway side is increased by 4.2 MPa (~40% increase). The peak value on the gob-side increases from 15.9 MPa to 22.8 MPa. Deformation of the surrounding rock in this special failure section increased compared with only the 051604 goaf influence. The anchor cable approaches failure under these stress conditions.

Therefore, we can see that the natural pressure relief process requires significant time after upper coal seam mining when the coal seams are separated by 21 m, thus the principal stress difference is not large on the roof and virgin coal. However, destruction of the coal pillar should not be disregarded. In order to prevent stress on the roof and two ribs of the roadway from increasing while mining the working face, reinforcements should be installed in the special section during mining.

4.2.3. Influence of 051606 Working Face Mining. After excavation of the 051606 ventilation roadway, the surrounding rock in the special failure section is relatively broken under the influence of the upper pillar. Some anchor cables are broken, and some anchor plates slip and fail. Therefore, we should improve the mechanical properties of the supporting structure and stress state of the surrounding rock, which can enhance the carrying capacity and meet the stability requirements during mining. Determining the supplement supporting parameters should also fully consider the later mining-induced stress influence. Under the mining influence, the special failure section will inevitably experience larger deformation due to the superposition of multiple stress fields. This will greatly affect the ventilation and pedestrian function of this roadway and even lead to mining accidents, such as the large-scale roof collapse. Therefore, it is very important to fully understand the deformation mechanism of the roadway due to mining-induced stress in the 051606 working face.

To research the superposition effect of mining on the special failure section as the 051606 working face advances, we should fully consider the influence of the upper pillar using the semiplane theory. The distances between the working face end and the edge of upper boundary pillar were set to 24, 16, 8, 0, −8, and −17.5 m (middle position of the pillar). The profile along the roof of the 051606 roadway is shown in Figure 10. We consider advance of the face end to the middle of the upper pillar as the length is changed. The stress on the rock surrounding the ventilation roadway is activated again by the side abutment pressure, and shear dilatancy failure of rock mass is the most serious when the face end is pushed to the middle position of the pillar (see Figure 10(f)).

The dynamic progress of the working face shows the following:

(1) In the 20 m section of the coal pillar, stress near the 051604 goaf side is more concentrated, and the maximum principal stress difference reaches 25 MPa. The cracks in this part are more developed and fragmented. Meanwhile, the principal stress difference near the ventilation roadway side is reduced to 8 MPa, and the stress reduction is as high as 68%. One can see that the integrity of this coal pillar section increases gradually from the 051604 gob-side to the ventilation roadway side. At this time, the middle of the coal pillar cannot form an effective elastic core area to maintain the stability of the coal pillar. Furthermore, based on the interaction between coal pillar failure and the surrounding rock stability of the gob-side roadway,

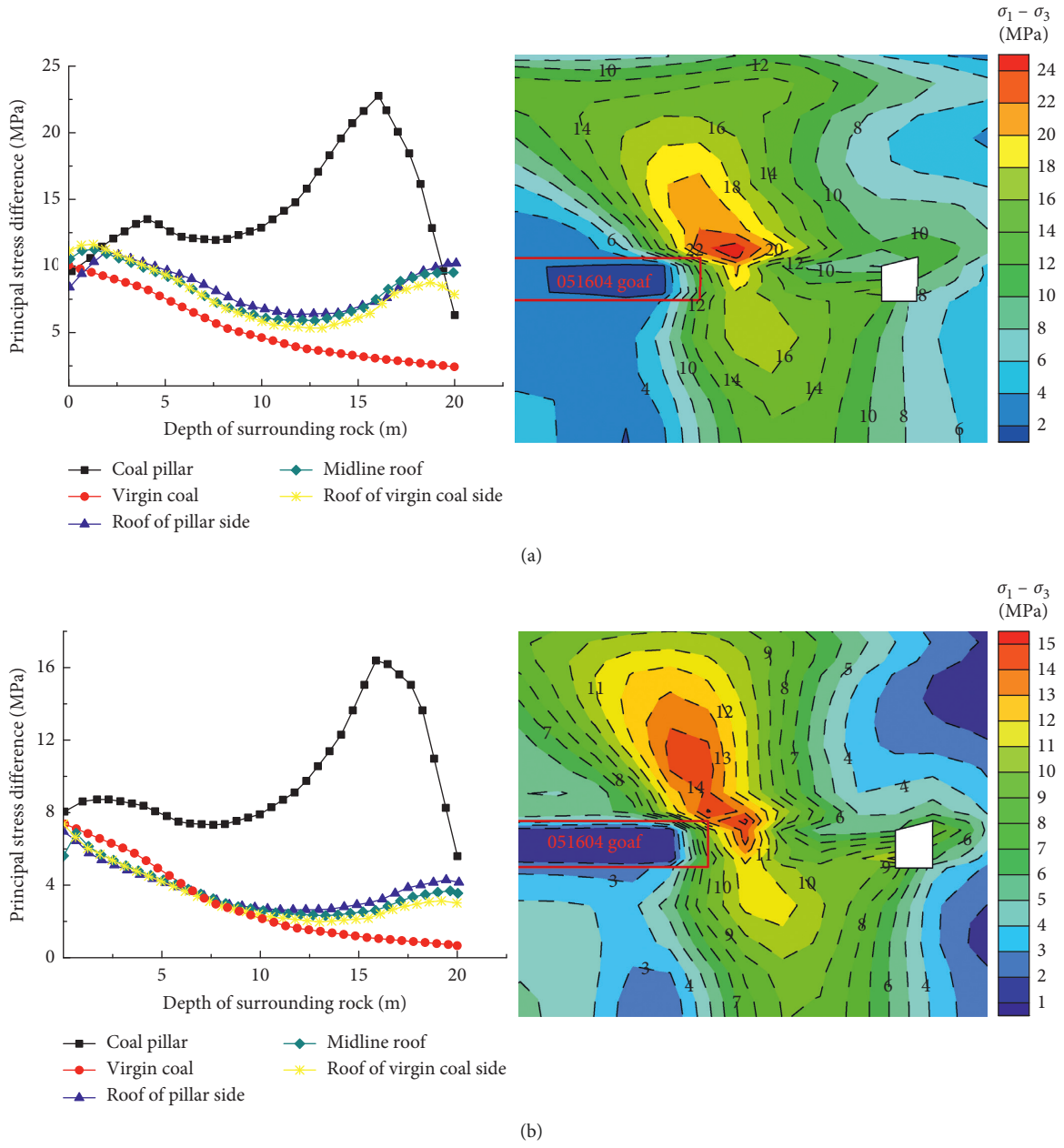

Figure 9: Principal stress difference distribution between single and double layer mining. (a) #15 coal seam in exploited conditions. (b) #15 coal seam in unexploited conditions.

the stress environment of the surrounding rock in this special failure section is not ideal.

(2) When the face end is 24 and 16 m away from the edge, stress fluctuations on the roadway roof in the special failure section are not great as mining advances from the face end to the edge of the upper boundary pillar. However, the roof stress increases obviously when the face end is 8 m from the edge of the upper pillar. It is concluded that the advance abutment pressure begins to affect this roadway section when the face end is about 16 m from the upper pillar. This stage is called the nonstress influence section. Subsequently, during advance from 16 to 0 m, the low stress range in the 20 m coal pillar on the ventilation roadway side decreases greatly, which directly affects the integrity of the coal pillar and seriously deteriorates roof stress in the special failure section. The maximum principal stress difference on the roof reaches 13 MPa. This stage is called the advance stress influence section. As the face end advances from the edge to the midline of the boundary pillar, the value and range of the principal stress difference in this roadway roof section increases further, and its influence is obviously stronger than that in the previous stage due to stress superposition from mining and the upper pillar. This

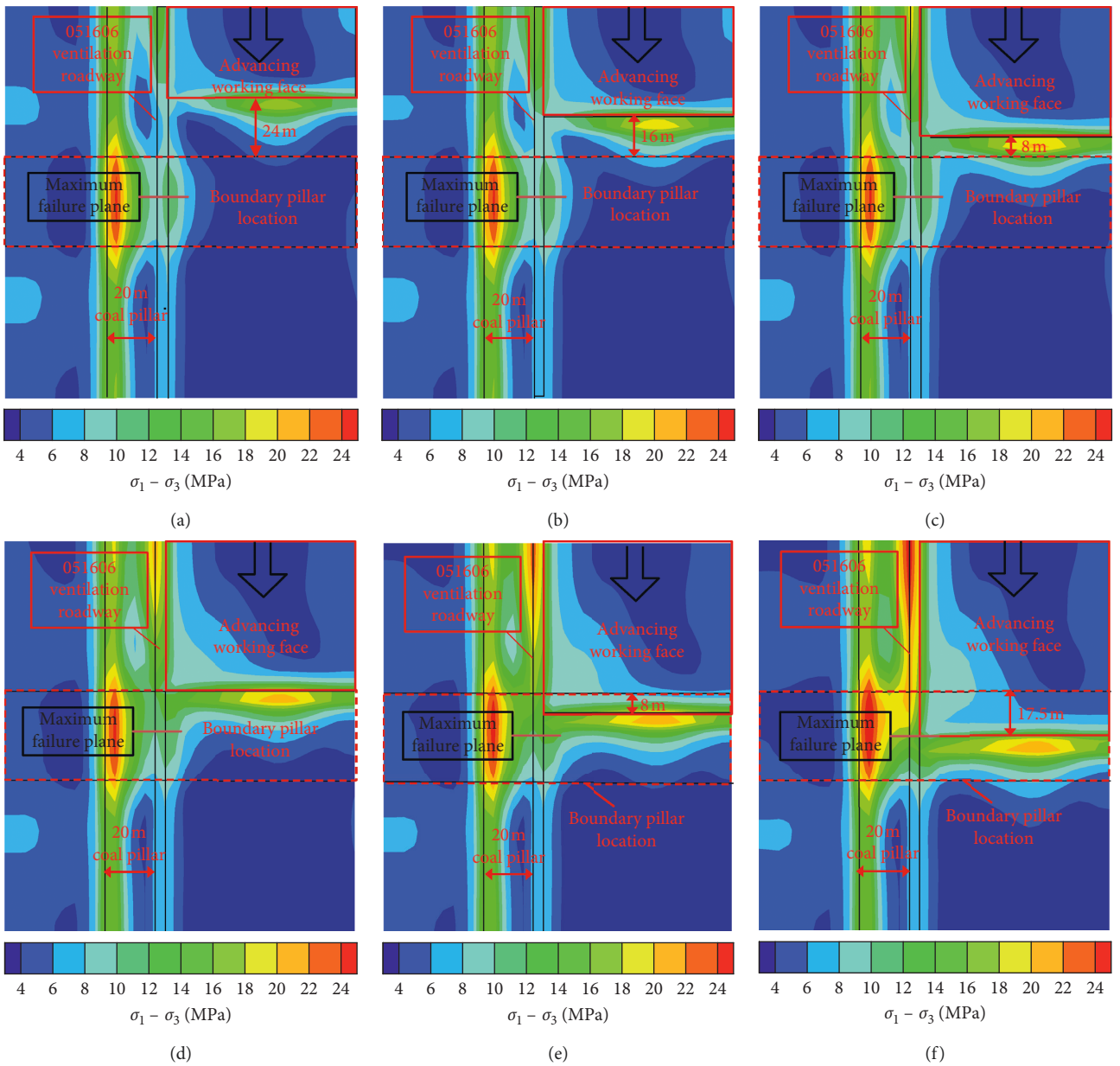

Figure 10: Stress state on rock surrounding vents while advancing the working face. (a) 24 m from face end to pillar. (b) 16 m from face end to pillar. (c) 8 m from face end to pillar. (d) 0 m from face end to pillar. (e) −8 m from face end to pillar. (f) −17.5 m from face end to pillar.

stage is called the superimposed stress influence section. Furthermore, the stability of the surrounding rock in the special failure section decreases greatly as the stress increases from 11 MPa to 18 MPa. At this time, when the working face advances to the midline position of the upper boundary pillar, the principal stress difference of the rock surrounding the roof reaches its peak value.

In summary, according to the influence of the mining process on the special failure section, the advancing process can be divided into three stages: the nonstress influence section (24 m to 16 m from the coal pillar), the advance stress influence section (16 m to 0 m from the coal pillar), and the superimposed stress influence section (from 0 m to −17.5 m from the coal pillar). These three stages are summarized in Table 2.

4.3. Analysis of Pressure in the Special Failure Section. Destruction of the surrounding rock in the ventilation roadway can be divided into three parts based on an analysis and comparison of the roadway damage during different impact stages. The first is the stress impact stage from the upper boundary pillar, the second is the influence of mining the 051604 adjacent working face, and the third is a secondary mining effect on the 051606 working face. The stress changes during these different stages are summarized in Table 3.

The rock surrounding the 051606 roadway roof suffers strong support pressure that is transmitted along the floor of

Table 2: Three stages of stress change during advance.

	Unstressed influence section	Advance stress influence section	Superimposed stress influence section
Roof stress in maximum failure plane (MPa)	10	11	18
Peak stress of roadway roof (MPa)	10	13	18
Peak position (m)	−17.5	0	−17.5

Table 3: Analysis of principal stress difference on the rock surrounding the roof during failure.

	Influence of boundary pillar	Influence of the 051604 working face	Influence of the 051606 working face
Influence value of each stage (MPa)	4.4	5.6	8
Total impact value (MPa)	4.4	10	18
Influence degree	Strong	Stronger	Extremely strong

the upper pillar. The peak principal stress difference in the special failure section is basically located at the midline position of the upper pillar. During adjacent working face mining, the peak principal stress difference in the roof of the special failure section reaches 10 MPa, and the stress environment of the surrounding rock deteriorated further. Subsequently, the integrity of the surrounding rock is significantly reduced while mining the 051606 working face. When the face end is located at the middle of the upper pillar (see Figure 10(f)), shear failure is most likely to occur in the roof on the coal pillar side, and the principal stress difference reaches 18 MPa. The simulation results show that this may cause serious roof collapse if the serious stress environment is not improved as the working face advances.

5. Surrounding Rock Control Technology

5.1. Difficulties in Surrounding Rock Control. According to damage from superimposed stress on the rock surrounding the ventilation roadway, the pedestrian and ventilation function can be maintained if the following three points are considered.

5.1.1. Asymmetric Zone Caused by Roadway Section Features. The 051606 ventilation roadway has a sloping roof with 3.32 m higher rib and 2.3 m lower rib. Under the influence of these features, the actual suspension length of the layered roof increases greatly when the roadway ribs are unstable. The suspension length of the higher rib support is significantly greater than that of the lower rib, resulting in a remarkable asymmetric stability distribution on the rock surrounding both sides of the roof. Furthermore, based on the interaction between the roof and the rock surrounding the two ribs, asymmetric damage on the roof rock mass will be superimposed on the high and low ribs. The higher rib will deform vertically, the lower rib will be removed, and the roof shoulder will bend asymmetrically.

5.1.2. Strengthening the Control Area. During excavation of the working face in the upper coal seam, the strata weight of the gob roof is transferred to the upper boundary pillar through the arch structure. According to the semiplane theory, stress diffuses along the floor of the coal pillar to the lower coal seam. Determining reasonable roadway protection is a major difficulty.

5.1.3. Second Mining-Induced Stress Activates the Original Stress Environment. The bedrock of the upper coal pillar is affected by the high support pressure, which is transmitted by the overlying coal pillar, and roadway excavation in this high stress region will cause a rapid release of vertical stress on the roadway roof. Meanwhile, stress concentration in the shoulders and ribs of the roadway will increase [26]. The surrounding rock stress environment is activated again after secondary mining of the working face, forming more intense strata behavior.

5.2. Support Parameters of Surrounding Rock. Strata behaviors are objective natural phenomena. It is impossible to completely eliminate strata behaviors during mining [15]. Therefore, under the premise of mine production safety, theoretical analysis and numerical simulation in FLAC3D were used to comprehensively determine the dynamic damage process and stress distribution on the upper boundary pillar and the lower ventilation roadway. At last, combined with the particularity of roadway section shape, the most scientific roadway support scheme is selected.

#15 coal seam is a monoclinic structure with an average inclination of 116°, while the 051606 roadway is designed as a special-shaped rectangular roadway with a higher rib height of 3.32 m, lower rib height of 2.3 m, and intermediate height of 2.81 m, with net cross sectional area is 13.49 m^2. This roadway uses a new form of support based on the highly stressed bolting support and anchor cable. This assists the steel ladder beam, steel mesh, and shed support in protecting the roof and ribs of the roadway. The specific support scheme is shown in Figure 11.

The roof bolting support includes a $\varphi 20 \times 2500$ mm left-handed and nonlongitudinal rebar threaded steel bolt. The row and line spacing is 770×900 mm, and each row is arranged with 7 anchor bolts. The bolts connecting the two ribs and roof form a 60° angle, and the other bolts are

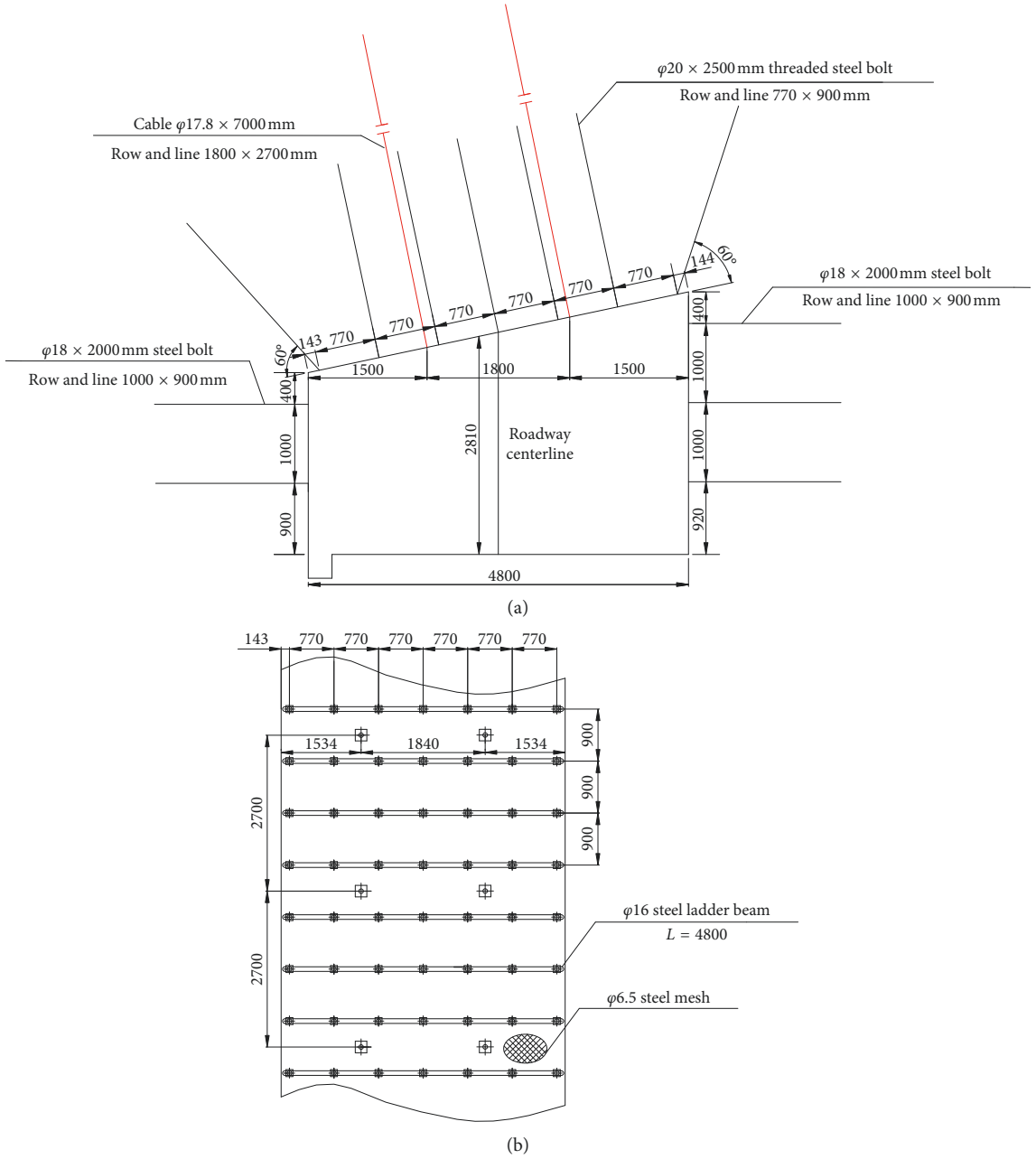

Figure 11: 051606 ventilation way supplement support scheme. (a) Elevation view of support scheme. (b) Horizontal projection of support scheme.

arranged vertically. The steel ladder beam is made of φ16 mm round welded steel beams 4800 × 80 mm in size. Each anchor cable measures φ17.8 × 7000 mm, and two anchor cables are used in each row. The row and line space is 1800 × 2700 mm, and the two anchor cables are arranged vertically on the roof. There are three bolts in the high rib and two bolts in the low rib. These are φ18 × 2000 mm steel bolts and are perpendicular to the ribs with row and line spacing of 1000 × 900 mm. According to the shape of the section, the heights of the shed legs are 2.4 m and 3.4 m. The two shed legs are embedded 100 mm in floor, and the shed beam is 4.9 m.

This scheme uses high stressed bolts (cable), a steel ladder beam, steel mesh, and shed for support. This composite beam structure is formed by the interaction between the bolt and shallow surrounding rock with the anchor cable and overlying hard main roof as the suspending structure. The roadway support asymmetry effectively reduces the bearing area. In addition, the strong protective ability of the steel mesh and shed support can better control the dilatancy deformation in the shallow surrounding rock. With this support method, the residual strength of the surrounding rock has increased. The surrounding rock and the supports form an effective bearing

structure, which greatly reduces or even prevents large deformation in the surrounding rock.

6. Control Effect of Strengthening Support

During actual mine construction, the 051606 roadway crosses through the upper boundary of the coal pillar in space. This roadway should be strong enough to support driving. The surrounding rock in the special failure section provides this functionality. The coal mass on the roof exhibits layered slippage, the coal mass in the rib shoulder falls and bulges to form a string bag, and more damage accumulates in the higher rib than in the lower rib. Therefore, it is possible to adopt emergency measures for supporting reinforcement after excavation proceeds for 10 days. Roof, floor, and rib displacement can be subsequently measured using the crossing method in this special failure section. The rock deformation curve is shown in Figure 12.

One can see that stabilization of the surrounding rock after excavation is a dynamic process until equilibrium is reached [27]. Roof deformation tends to become stable about 20 days after implementing supports, and the two ribs and floor rock become stable after about 15 days. Stress in the surrounding rock can stabilize after a short time. The maximum convergence of roof rock is approximately 200 mm, and the minimum floor convergence is only about 100 mm. The maximum convergence between the roof, floor, and ribs due to mining-induced stress is about 300 mm. According to the relationship between the support structure and the surrounding rock, design of the roadway support based on a controlled load is not suitable, thus controlled deformation should be used. Therefore, although the rock surrounding the roadway experiences some deformation to a certain extent under the influence of strong stress, the basic ventilation and pedestrian functions will not be directly lost if the roadway is maintained by reasonable supporting forms. It can be also seen that this reinforcing support can protect the roof and ribs, while the surrounding rock has also reached an internal balance after a relatively short period of time. We find that the reinforcing support method has a more remarkable effect on roadway maintenance.

7. Conclusions

This study uses the methods of theoretical analysis, FLAC numerical simulation, and engineering practice to obtain the following conclusions:

(1) Semiplane theory can be used to deduce and mathematically calculate the stress distribution on the floor. Furthermore, the principal stress difference is introduced into this solution model. It is concluded that the stress distribution under this condition exhibits fan-shaped diffusion. The stress distribution on #16 coal seam roof has a single peak. The maximum failure plane is located in the middle of the upper coal pillar. Finally, we found that the strengthening control area in the 051606 ventilation roadway is 45 m from the change point position on #16 coal seam roof.

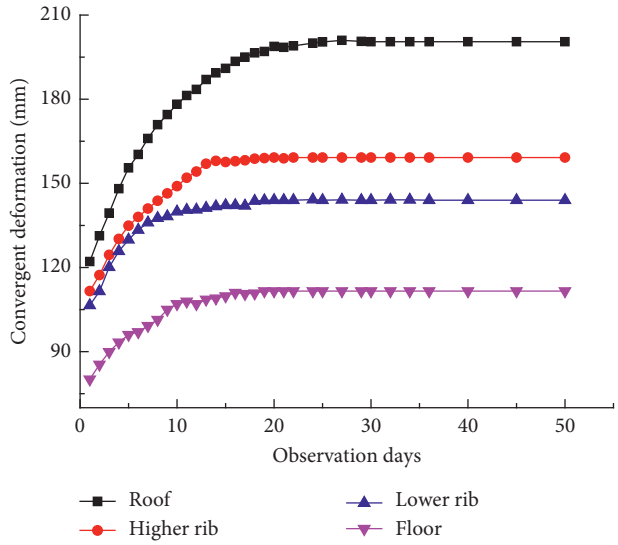

Figure 12: Strata behavior curve.

(2) FLAC3D was used to successively simulate the influence of the upper boundary pillar, the 051604 gob, and the 051606 working face. It is concluded that mining the 051606 working face is the greatest determinant of stability of the rock surrounding the roadway, followed by mining the 051604 working face.

(3) The principal stress difference distribution in the rock surrounding the special failure section exhibits obvious asymmetric characteristics. Therefore, an asymmetric support form is proposed that uses highly stressed bolts, an anchor cable, steel ladder beam, steel mesh, and a shed to add support to the roof and ribs of the roadway. This support structure was successfully applied in a real project.

Data Availability

All data supporting the conclusions drawn by this study can be obtained from the corresponding author upon request.

Disclosure

The funders had no role in the design of the study; in the collection, analyses, or interpretation of data; in the writing of the manuscript; and in the decision to publish the results.

Conflicts of Interest

The authors declare that there are no conflicts of interest.

Authors' Contributions

Zheng Zheng conceived and designed the paper. Fulian He, Hengzhong Zhu, and Bo Yang analyzed the data. All authors have written, reviewed, and approved the final manuscript.

Acknowledgments

This project was supported by the National Natural Science Foundation of China (no. 51574243), by the Yue Qi Distinguished Scholar Project (800015Z1138), China University of Mining & Technology, Beijing, and also by the Fundamental Research Funds for the Central Universities (800015J6).

References

[1] L. Yuan, "Key technique of safe mining in low permeability and methane-rich seam group," *Chinese Journal of Rock Mechanics and Engineering*, vol. 27, pp. 1371–1378, 2008.

[2] C. F. Yuan, "Development and application of gas-geology in China," *Journal of China Coal Society*, vol. 22, pp. 566–570, 1997.

[3] Y. P. Cheng and Q. X. YU, "Development of regional gas control technology for Chinese coalmines," *Journal of Mining and Safety Engineering*, vol. 24, no. 10, pp. 383–390, 2007.

[4] F. P. Gong and X. B. Li, "Catastrophe progression method for stability classification of underground engineering surrounding rock," *Journal of Central South University of Technology*, vol. 39, pp. 1081–1086, 2008.

[5] W.-Y. Guo, T.-B. Zhao, Y.-L. Tan, F.-H. Yu, S.-C. Hu, and F.-Q. Yang, "Progressive mitigation method of rock bursts under complicated geological conditions," *International Journal of Rock Mechanics and Mining Sciences*, vol. 96, pp. 11–22, 2017.

[6] W. Y. Guo, Y. L. Tan, and F. H. Yu, "Mechanical behavior of rock-coal-rock specimens with different coal thicknesses," *Geomechanics and Engineering*, vol. 15, no. 4, pp. 1017–1027, 2018.

[7] J. W. Cassie and P. B. Cartwright, "Coal pillar behavior from underground stress measurements," in *Proceedings of 9th International Congress on Rock Mechanics*, pp. 1347–1354, Paris, France, August 1999.

[8] J. K. Jiao and W. J. JU, "Multi-factors analysis of the stability of roadway under coal pillar based on response surface method," *Journal of Mining and Safety Engineering*, vol. 34, pp. 933–939, 2017.

[9] S. L. Lu and L. Y. Sun, "Selection of horizontal distance X between roadway and the edge of its upper pillar," *Journal of China University of Mining & Technology*, vol. 22, pp. 1–7, 1993.

[10] S. L. Lu and Y. D. Jiang, "The selection of vertical distance Z between roadway and its upper coal seam," *Journal of China University of Mining & Technology*, vol. 22, pp. 1–7, 1993.

[11] Y. B. Guan and H. M. Li, "Research of No19coal seam floor's fracture regularity in Xiandewang Coal Mine," *Journal of China Coal Society*, vol. 28, pp. 121–125, 2003.

[12] Y. Zhang and C. L. Zhang, "The study on roadway layout in coordination of mining coal seams base on failure of floor strata," in *Engineering Solutions for Manufacturing Processes IV, pts 1 and 2*, Z. Jiang, X. Liu, and J. Han, Eds., vol. 889-890, pp. 1362–1374, Trans Tech Publications Ltd, Stafa-Zurich, Switzerland, 2014.

[13] A. H. Wilson, "The stability of underground workings in the soft rocks of the Coal Measures," *International Journal of Mining Engineering*, vol. 1, pp. 91–187, 1983.

[14] L. Xu and H. L. Zhang, "Principal stress difference evolution in floor under pillar and roadway layout," *Journal of Mining and Safety Engineering*, vol. 32, pp. 478–484, 2015.

[15] W. Li, J. Bai, S. Peng, X. Wang, and Y. Xu, "Numerical modeling for yield pillar design: a case study," *Rock Mechanics and Rock Engineering*, vol. 48, no. 1, pp. 305–318, 2014.

[16] W. Sui, Y. Hang, L. Ma et al., "Interactions of overburden failure zones due to multiple-seam mining using longwall caving," *Bulletin of Engineering Geology and the Environment*, vol. 74, no. 3, pp. 1019–1035, 2014.

[17] W. B. Zhu, *Study on the Instability Mechanism of Key Strata Structure in Repeat Mining of Shallow Close Distance Seams*, China University of Mining and Technology, Xuzhou, China, 2010.

[18] J. Qiao, "On the preimages of parabolic periodic points," *Nonlinearity*, vol. 13, no. 3, pp. 813–818, 2000.

[19] J. Y. Qiao, *Complex Dynamics of Renormalization Transformations*, Science Press, Beijing, China, 2010, in Chinese.

[20] Z. G. Xu, *Elasticity*, Higher Education Press, Beijing, China, 2006.

[21] M. G. Qian and P. W. Shi, *Kuangshan Yali Yu Yanceng Kongzhi*, China University of Mining and Technology Press, Xuzhou, China, 2010.

[22] B. Yu and Y. C. Liu, "Mechanism of strong pressure reveal under the influence of mining dual system of coal pillar in Datong mining area," *Journal of China Coal Society*, vol. 39, pp. 40–46, 2014.

[23] G. X. Li and B. Y. Zhang, *Soil Mechanics*, Tsinghua University Press, Beijing, China, 2013.

[24] G. Zhang, S. Liang, Y. Tan, F. Xie, S. Chen, and H. Jia, "Numerical modeling for longwall pillar design: a case study from a typical longwall panel in China," *Journal of Geophysics and Engineering*, vol. 15, no. 1, pp. 121–134, 2018.

[25] B. S. Zhang, S. S. Yang, and L. X. Kang, "Discussion on method for determining reasonable position of roadway for ultra-close multi-seam," *Chinese Journal of Rock Mechanics and Engineering*, vol. 27, pp. 97–101, 2008.

[26] X. G. Su, X. M. Song, and H. H. Yuan, "Stability control of the roadway group under the influence of overlying goaf," *Journal of Mining and Safety Engineering*, vol. 33, pp. 415–422, 2016.

[27] K. X. Zhang, Y. J. Zhang, and Z. Q. Ma, "Determination of the narrow pillar width of gob-side entry driving," *Journal of Mining and Safety Engineering*, vol. 32, pp. 446–452, 2015.